High-Resolution Nonlinear Optical Imaging of Live Cells by Second Harmonic Generation

Paul J. Campagnola,* Mei-de Wei,* Aaron Lewis,# and Leslie M. Loew*
*Department of Physiology and Center for Biomedical Imaging Technology, University of Connecticut Health Center, Farmington, Connecticut 06030 USA, and #Division of Applied Physics, Hebrew University, Jerusalem, Israel

ABSTRACT By adapting a laser scanning microscope with a titanium sapphire femtosecond pulsed laser and transmission optics, we are able to produce live cell images based on the nonlinear optical phenomenon of second harmonic generation (SHG). Second harmonic imaging (SHIM) is an ideal method for probing membranes of living cells because it offers the high resolution of nonlinear optical microscopy with the potential for near-total avoidance of photobleaching and phototoxicity. The technique has been implemented on three cell lines labeled with membrane-staining dyes that have large nonlinear optical coefficients. The images can be obtained within physiologically relevant time scales. Both achiral and chiral dyes were used to compare image formation for the case of single- and double-leaflet staining, and it was found that chirality plays a significant role in the mechanism of contrast generation. It is also shown that SHIM is highly sensitive to membrane potential, with a depolarization of 25 mV resulting in an approximately twofold loss of signal intensity.

INTRODUCTION

In this paper we describe the use of surface second harmonic generation (SHG) in laser scanning microscopy as a new contrast mechanism for live cell imaging. SHG is a second-order nonlinear optical process and thus requires an environment without a center of symmetry, such as an interfacial region, to produce a signal. Over the last two decades SHG has been widely used as a spectroscopic tool in a variety of interfacial studies, including liquid-solid, liquid-air, and liquid-liquid interfaces (Shen, 1989). Applications have included probing equilibrium properties such as absolute orientation of molecules at surfaces, structural phase transitions, and electrochemical potential. This methodology has also been used to study dynamic interfacial processes, including photoisomerization of organic molecules and adsorption kinetics. Eisenthal provides an excellent overview of the scope of recent work (Eisenthal, 1996). Many of the approaches used to probe bulk interfacial properties can be extended to microscopy. This idea was first demonstrated in the 1970s by Hellwarth and Christensen (Hellwarth, 1974) and Sheppard (Sheppard et al., 1977) and again more recently (Gauderon et al., 1998). Because of the interfacial specificity of the process, SHG is an ideal approach to the study of biophysics in model membranes (Huang et al., 1988; Bouevitch et al., 1993) and the membrane physiology of living cells (Ben-Oren et al., 1996; Peleg et al., 1999; Lewis et al., 1999).

We begin with an overview of the physical background of nonlinear optical processes. In general, the nonlinear polarization for a material can be expressed as

$$P = \chi^{(1)}E^1 + \chi^{(2)}E^2 + \chi^{(3)}E^3 + \cdots \quad (1)$$

where P is the induced polarization, $\chi^{(n)}$ is the nth-order nonlinear susceptibility, and E is the electric field vector. The first term describes normal absorption and reflection of light; the second, SHG, sum and difference frequency generation; and the third, light scattering, stimulated Raman processes, third harmonic generation, and both two- and three-photon absorption. The processes of two-photon excited fluorescence (TPEF) and second harmonic generation are shown in the Jablonsky diagram in Fig. 1. In two-photon absorption, a fluorophore is simultaneously excited from the ground state, S_0, through a virtual state to either the first or second excited sates, S_1 or S_2, respectively. In the latter case rapid nonradiative (1-ps) decay to S_1 generally results in the same emission independent of excitation mode. SHG, in contrast, does not arise from an absorptive process. Instead, an intense laser field induces a nonlinear polarization in a molecule or assembly of molecules, resulting in the production of a coherent wave at exactly twice the incident frequency. The magnitude of the SHG wave can be resonance enhanced when the energy of the second harmonic signal overlaps with an electronic absorption band (Heinz et al., 1982). Here the total second-order response is a sum of the nonresonant and resonant contributions:

$$\chi^{(2)}_{\text{total}} = \chi^{(2)}_{\text{nonres}} + \chi^{(2)}_{\text{res}} \quad (2)$$

where the latter term arises from a sum over states expression. Depending on the specific properties of the chromophore, the resonant contribution can dominate, resulting in enhancement of an order of magnitude or more.

A major constraint of SHG is the requirement of a noncentrosymmetric environment. This is readily understood by inspection of Eq. 1. The SHG wave is a vector quantity, and within the electric dipole approximation, the induced

Received for publication 14 April 1999 and in final form 16 August 1999.
Address reprint requests to Dr. Paul Campagnola, Department of Physiology, University of Connecticut Health Center, 263 Farmington Ave., Farminton, CT 06030-3505. Tel.: 860-679-4354; Fax: 860-679-1269; E-mail: campagno@panda.uchc.edu.

0006-3495/99/12/3341/09 $2.00

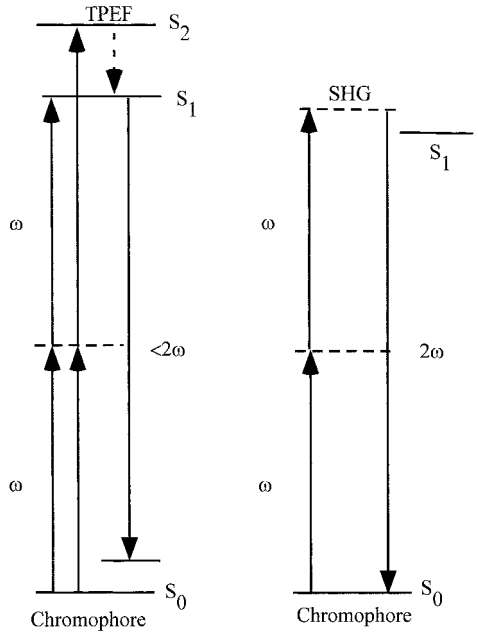

FIGURE 1 Jablonksy diagram comparing the photophysical pathways for two-photon excited fluorescence (*left*) and resonance enhanced second harmonic generation (*right*).

polarization in a centrosymmetric sample from one direction would be equal to and opposite the other, thus canceling. Because of the inherent asymmetry of lipid bilayers, both intracellular organelle and plasma membranes are suitable samples for probing with this methodology. This is because the membrane structure forces a noncentrosymmetric environment, provided only one leaflet is stained. Conversely, this technique is not amenable to probing cytosolic dynamics. SHG can also result from an electric quadrupole interaction from samples with a large change in optical dielectric constant between the interfacial regions. This interaction can also give rise to a SHG signal from centrosymmetric regions; however, this contribution is much weaker than interfacial components, and these effects are expected to be negligible in living cells.

Because SHG is a nonlinear optical phenomenon, it could form the basis of a high-resolution nonlinear optical imaging scheme that possesses all of the benefits of multiphoton excited fluorescence microscopy. There has been an explosion in the use of this technique since the first implementation in biological microscopy in 1990 (Denk et al., 1990). Because of greatly reduced out-of-plane photobleaching and phototoxicity, this methodology has gained considerable popularity as an ideal method for live cell imaging. In part this growth has occurred because of the large advances in mode-locked laser technology, namely the advent of titanium sapphire as a femtosecond lasing medium. This technique has proved useful in neuroscience, cell biological, and biophysical applications (Denk et al., 1990, 1995; Maletic-Savatic et al., 1999; Potter et al., 1996; Maiti et al., 1997). Popular implementations have been in green fluorescent protein (GFP) imaging (Niswender et al., 1995; Patterson et al., 1997; Potter et al., 1996) and imaging in thick tissue and turbid media (Kleinfeld et al., 1998; Wokosin et al., 1996; Maletic-Savatic et al., 1999). The resolution demonstrated in multiphoton applications has been comparable to or slightly less than that achievable by ordinary confocal microscopy (Gu and Sheppard, 1995). However, following deconvolution, Hell and co-workers have demonstrated axial and lateral superresolution in two-photon 4π microscopy (Hell et al., 1997).

Despite all of these advantages new problems can arise from nonlinear optical schemes. Because of the high peak powers necessary for multiphoton absorption, undesired, toxic nonlinear optical effects can occur. These effects include accidental three-photon absorption of nucleic acids and proteins and formation of destructive plasma. Furthermore, in-plane absorption and eventual photobleaching still generate toxic free radicals in the same manner as one-photon excitation. Gratton and co-workers (König et al., 1997, 1999) have determined acceptable exposure limits in Chinese ovarian hamster cells by monitoring cell division. Because SHG does not arise from absorption, in-plane photobleaching and phototoxicity of labeling fluorophores can be greatly reduced if the laser wavelength is off resonance. Furthermore, because it is not necessary to match the excitation wavelength to a given fluorophore, it is possible to image further into the infrared (e.g., $\lambda > 900$ nm), avoiding most endogenous two- and three-photon UV absorption and thus minimizing cell damage. However, in the current work, which was performed at 880 nm, the observed SHG signals were resonance enhanced to increase signal-to-noise ratios, and phototoxic effects were thus expected to be comparable to those observed in multiphoton excitation schemes.

In the first biologically relevant SHG experiment (Bouevitch et al., 1993) SHG was demonstrated in a model membrane stained with a voltage-sensitive dye on a hemispherical bilayer apparatus. More recently low-resolution SHG imaging (SHIM) was used to monitor slow membrane potential responses after stimulation of photoreceptor cells by visible light (Ben-Oren et al., 1996). Here we demonstrate that by scanning a short pulse laser an SHG image with a pixel density similar to that of confocal microscopy can be acquired on physiologically relevant time scales. Images have been obtained for N1E-115 neuroblastoma cells, National Institutes of Health (NIH) 3T3 fibroblasts, and L1210 lymphocytes. For increased contrast, the cells are stained with potential-sensitive dyes that have chromophores with large second-order optical nonlinearities. The mechanisms and efficiency of contrast generation in these cells have been elucidated using different dyes that consist of the same styryl chromophore but have different alkyl chain lengths and chiralities. The structures of these dyes are shown in Fig. 2, *a–d*. In particular, we used these variants to examine the cases of single- and double-leaflet staining as well as to determine the enhancement of the SHG signal due to the presence of a chiral center. We demonstrate how laser scanning SHIM can be used to monitor membrane potential with much greater sensitivity

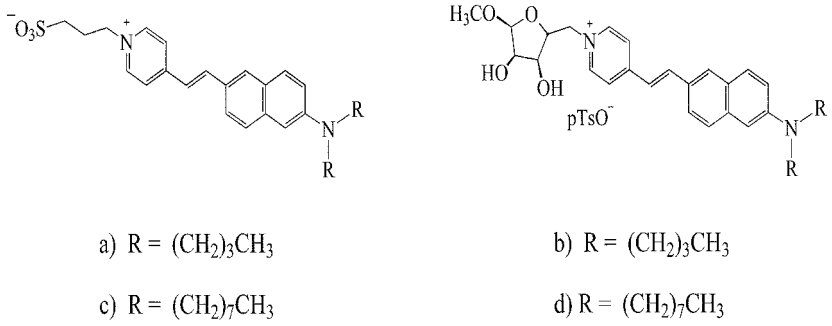

FIGURE 2 Structures of membrane staining styryl dyes used for cell labeling. (*a*) di-4-ANEPPS, (*b*) chiral JPW-1259, (*c*) di-8-ANEPPS, (*d*) chiral JPW-2080. The chromophore is the same for all four molecules.

than possible via fluorescence imaging. We also discuss the effects of sample size on SHG image formation.

EXPERIMENTAL METHODS

Microscope and laser

The SHIM experiments were performed on a modified Biorad MRC600 scan head on an upright microscope, the optical path of which is shown in Fig. 3. The laser system is a Coherent argon ion (Innova 310) pumped femtosecond titanium sapphire oscillator (900-F), characterized by a pulse width of ~100 fs at a repetition rate of 76 MHz at 880 nm. Average powers at the sample were between 5 and 50 mW. Because SHG is a coherent process, the signal wave copropagates with the laser and is collected in a transmitted light configuration. Matching 1.3 N.A. oil immersion objectives (Zeiss, Fluar) are used for excitation and signal collection. The 1-mrad divergence of the Ti:sapphire laser was compensated before the scan head. There is essentially no dispersion at 880 nm, and thus no external precompensation was used to compensate for the minimal group delay in the scan head or objective. Because at the fundamental excitation wavelength there is considerable resonance enhancement, the TPE fluorescence can be simultaneously collected on one of the Biorad fluorescence channels. The fluorescence signal is descanned and collected with the pinhole aperture fully opened.

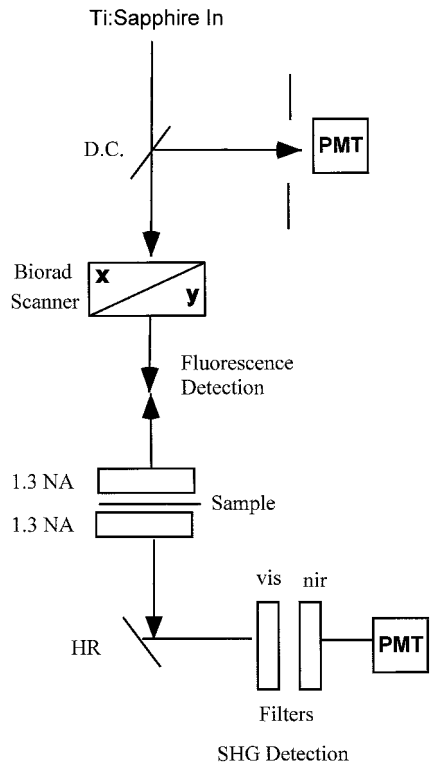

FIGURE 3 Optical schematic of the SHG/TPEF microscope. The TPEF is descanned and collected with the pinhole fully open. The SHG is collected in a transmitted light configuration and isolated with optical filters. Use of a matching collection objective resulted in larger collection efficiency than was observed with a high N.A. condenser. The signal is detected with a hybrid single photon counting/analog integration scheme and integrated by the Biorad MRC600 electronics.

The transmitted light consisting of the fundamental laser (880 nm), TPE fluorescence (max 650 nm), and the SHG (440 nm) is recollimated and directed into the photomultiplier tube (PMT) (Hammamatsu 4632). Color glass (Schott BG-39) filters and a 500-nm shortwave pass filter attenuate the laser fundamental and TPE fluorescence, respectively. A hybrid of single-photon counting and analog integration was implemented to increase the signal-to-noise ratio of the second harmonic images. The photomultiplier is operated in single-photon counting mode and run through a 5× preamplifier (Stanford Research Systems SR445). The single counts were discriminated using a 200-MHz photon counter (Stanford Research Systems SR400). The resulting NIM pulses were converted to TTL with a level converter (Phillips Scientific 726) and made of equal duration with a gate and delay generator (Berkely Nucleonics 8010). The width and amplitude of these pulses were adjusted to use the entire dynamic range of the Biorad integrator. Detected signals consisted of 5–15 photons for 1.6-μs pixel dwell times. Typical data are the result of three to five Kalman averages and thus require a total acquisition time of 3–5 s to reduce high-frequency background light levels.

Spectroscopic measurements on suspended cells

In addition to imaging experiments, ensemble-averaged spectroscopic measurements were performed on suspended L1210 cells. These were used to determine the SHG enhancement due to chirality in the styryl dyes as well as to determine the sensitivity of the SHG signal to membrane potential. A block diagram of the apparatus is shown in Fig. 4. The laser fundamental wavelength for these measurements was 800 nm. The second harmonic and TPE fluorescence signals were produced and collected with 5 × 0.15 N.A. (Zeiss) and 5 × 0.25 N.A. (Zeiss) objectives, respectively, dispersed through a 0.25-m monochromator, and detected with a Hammamatsu R4632 PMT equipped with a BG-39 glass filter to eliminate spurious signal at 800 nm arising from the second order of the grating. The resulting signal was preamplified (Stanford Research Systems SR445) and integrated with a boxcar averager (Stanford Research Systems model 250). To compensate for fluctuations of cell density and staining concentration within and between preparations of differing conditions, the SHG signal was normalized to the TPEF intensity at 560 nm. This color was detected with the maximum efficiency as a compromise between the emission spectrum (max 650 nm) and quantum efficiency of the PMT. Relative membrane potential measurements were determined in samples of normal buffer and high K^+ (135 mM). The SHG signals were then normalized to the fluo-

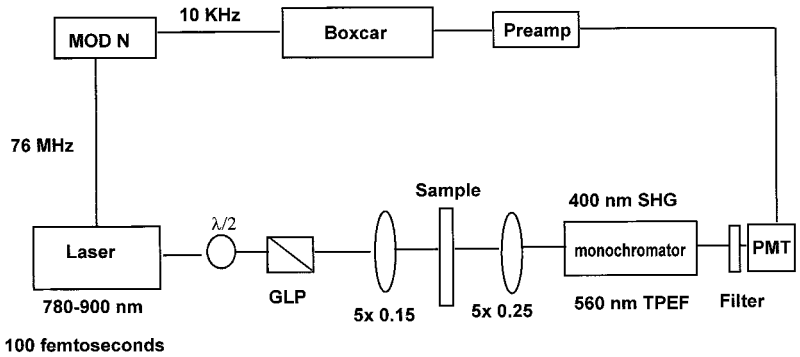

FIGURE 4 Optical schematic of spectroscopic SHG/TPEF measurements. The laser power is controlled with a halfwave plate and Glan-Laser polarizer. SHG (400 nm) and TPEF (560 nm) signals are dispersed with a ¼ meter monochromator, and the PMT is run through a 5× preamp and integrated by a boxcar synchronized to the laser pulse train, minimizing any possible jitter in the collection window. The maximum trigger rate of the boxcar is 10 kHz, and the trigger is provided by a Conoptics model 305 Mod N divider.

rescence signal, ignoring the small change in the latter (~10%) upon plasma membrane depolarization.

Cell preparations

NIH 3T3 cells were grown in Dulbecco's modified Eagle's medium (DMEM) supplemented with 10% fetal calf serum and maintained at 37°C with 5% CO_2. Subconfluent cultures were harvested by trypsinization (0.05% trypsin and 0.53 M EDTA). NIE-115 mouse neuroblastoma cells were grown in DMEM with 10% fetal calf serum and maintained at 37°C with 5% CO_2. After plating, differentiated cells were further treated with low serum (0.5% fetal bovine serum) and 1% dimethyl sulfoxide. L1210 cells were grown in DMEM with 10% horse serum and maintained at 37°C with 5% CO_2. All experiments were performed using EBBS containing additional 20 mM HEPES and adjusted to pH 7.4. Coverslips were incubated with dye solution (dye in EBBS containing 0.05% pluronic F-127) for 15 min at 10°C and then washed. Final dye concentrations were 1–5 μM. L1210 cells were centrifuged and resuspended in either EBBS or 1:1 EBBS and agarose, and the cell concentration was ~10^6/ml. Agarose was required to reduce the Brownian motion of the cells to permit a stable measurement.

Liposome preparation

Phosphatidylcholine vesicles at concentration of 10 mg/ml were prepared from crude soybean lecithin (type II) and K^+ pH 7.3 buffer containing 50 nM K_2SO_4, 1 mM EGTA, and 10 mM HEPES. The vesicles were vortexed for 10 min under argon, sonicated for 5 min, quick frozen in liquid N_2, thawed to room temperature, and resonicated. Dye (90 μM) was then added and samples were used immediately.

RESULTS

Enhancement of SHG due to chirality

The molecules shown in Fig. 2, *a* and *c*, di-4-ANEPPS and di-8-ANEPPS, respectively, were developed as potential-sensitive probes. The chiral sugar group in JPW-1259 (Fig. 2 *b*) and JPW-2080 (Fig. 2 *d*) was added specifically to enhance the second-order coefficient by increasing the molecular asymmetry. Typically $\chi^{(2)}$ values are determined by spin-casting dye onto a substrate, forming a monolayer. From the point of view of biophysics it is more relevant to make measurements in a biological membrane. Initial efforts were made in preparations of PC liposomes stained with di-4-ANEPPS (Fig. 2 *a*) and JPW-1259 (Fig. 2 *b*). While we observed efficient TPEF, these samples were unsuccessful in producing second harmonic signal. The physical basis for this observation will be explained in the Discussion. However, suspended L1210 lymphocytes proved to be convenient substrates for SHG.

To compare relative $\chi^{(2)}$ values, we exploit the fact that because the chromophores of these dyes are the same, they have indistinguishable TPE cross sections (data not shown). Therefore, we can use the TPE intensity to normalize the SHG intensity for varying stain levels, facilitating comparison of SHG for different dyes. Thus, using the apparatus shown in Fig. 4, we determined the relative $\chi^{(2)}$ values of the achiral (Fig. 2 *a*) and chiral (Fig. 2 *b*) dyes at 800 nm. These experiments determined the ratio of the chiral and achiral relative second-order nonlinear susceptibilities $\chi^{(2)}$ to be

$$\frac{\chi^{(2)}_{\text{chiral}}}{\chi^{(2)}_{\text{achiral}}} = \frac{\text{SHG/TPEF}_{\text{chiral}}}{\text{SHG/TPEF}_{\text{achiral}}} = 2.2 \pm 0.4 \qquad (3)$$

Imaging of neuroblastoma cells

Initial imaging experiments were performed on N1E-115 neuroblastoma cells. These tissue culture cells are convenient models for central nervous system neuronal cells and serve nicely to illustrate the power of SHIM. The fundamental excitation color (880 nm) is on the red edge of the two-photon absorption band, and there is sufficient TPEF to simultaneously collect these images. Because the TPEF and SHG signals are expected to arise from the same stain, this methodology provides a useful comparison between the techniques and a benchmark of performance of the contrast mechanism. Fig. 5, *a* and *b*, show the respective SHIM and TPEF images of undifferentiated and differentiated N1E-115 neuroblastoma cells, respectively, labeled with JPW-2080 (structure shown in Fig. 2 *d*). Inspection of these images indicates that these two modalities carry the same information, i.e., in both cases the signal appears largely at the plasma membrane with some internal staining. The two cells in Fig. 5 *b* show the common features of differentiated neuronal cells: the soma, neurites, growth cones, and filopodia are all apparent. Qualitatively, the resolution and contrast of TPE fluorescence and SHG are similar. Careful inspection of many data sets has revealed slight differences between the two contrast mechanisms at isolated regions of

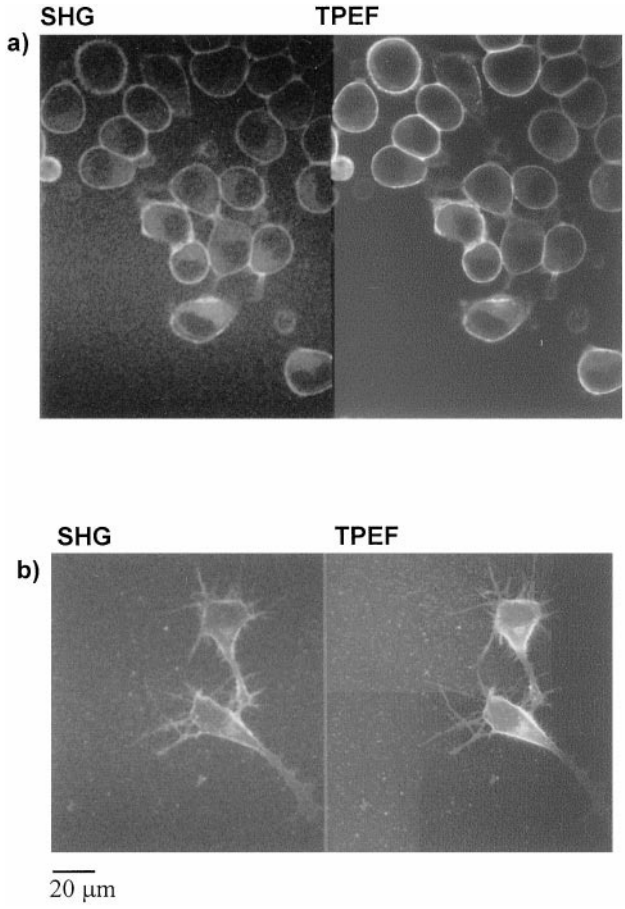

FIGURE 5 (*a*) SHG (*left*) and TPEF (*right*) images of undifferentiated N1E-115 neuroblastoma cells stained with JPW-2080. The power at the sample was ~10 mW, and the image is the result of five Kalman averages and a 5-s total acquisition time. (*B*) SHG (*left*) and TPEF (*right*) images of differentiated N1E-115 neuroblastoma cells stained with JPW-2080. The power at the sample was ~40 mW, and the image is the result of five Kalman averages.

these cells. It is unclear at this point if such differences are physiological or arise from other, as yet unknown, effects.

Several diagnostic controls were performed to ensure that the measured signal appeared only at the expected SHG wavelength and depended on the styryl dye. First, the Ti:sapphire laser was taken out of mode-locking operation and no SHG was observed, indicating that the signal arose from a nonlinear optical process. This is because when in continuous wave (cw) lasing mode, the Ti:sapphire has insufficient peak power to produce either TPEF or SHG with any measurable efficiency. Second, the transmitted light was dispersed through a 0.25-m monochromator, and while the associated losses prohibited imaging in this mode, the signal from a whole scan field was integrated and was observed only at the second harmonic wavelength. Furthermore, the signal had the expected spectral bandwidth of ~7 nm FWHM; the laser fundamental has a FWHM of ~10, and for a Gaussion profile, the bandwidth of the SHG signal scales as the square root of the fundamental bandwidth. In measurements on suspended L1210 cells, the laser was scanned between 800 and 900 nm, and the SHG signal did indeed track the fundamental laser color on a constant, near-zero background (data not shown). No fluorescence background was observed below 450 nm, demonstrating that the observed SHG signal was indeed free of fluorescent components. Last, cells with no staining produced no observable signal.

At this wavelength (880 nm), an average power of 50 mW was observed to bleach the dye after ~20 frames, but no obvious physical damage was observable. Some data were obtained with an average power of 10 mW, and under these conditions these live cells appeared photostable with respect to obvious photodamage and photobleaching. However, no assays such as monitoring cell division were performed. Conversely, initial experiments at 780 nm resulted in rapid, readily visible widespread cell damage, further demonstrating the importance of using long-wave excitation.

3T3 fibroblast imaging

Because cell membranes are bilayers, membranes are fundamentally a form of interface different from that typically studied by SHG. A central issue therefore is whether the signal can arise from dye labeling just the outer leaflet or labeling both leaflets of the plasma membrane equally. To investigate this question, we performed SHIM experiments on NIH 3T3 fibroblasts. These flat cells internalize membrane-staining dyes relatively rapidly, resulting in equal double-leaflet staining. Furthermore, the cells were stained with the shorter alkyl chain dyes di-4-ANEPPS (Fig. 2 *a*) and JPW-1259 (Fig. 2 *b*), which are known to internalize faster than the di-8 analogs (Loew, 1994). The SHIM and TPEF data for the JPW-1259 chiral dye are shown in Fig. 6, *a* and *b*, respectively. As with the two prior cell lines, the images are essentially identical, but now widespread internal membrane staining is also observed. Representative SHG and TPEF images of achiral di-4-ANEPPS-labeled cells are shown Fig. 6, *c* and *d*, respectively. Although the TPEF images were strong, no coherent SHG images were obtainable from this dye, suggesting a much stronger dependence on the presence of a chiral center than would be predicted from the relative $\chi^{(2)}$ values. The physical interpretation of this effect will be described in the Discussion.

Membrane potential measurements

A major goal of this work is to use SHG as a new method to probe physiology by measuring membrane potential. For fast membrane-staining potentiometric dyes, fluorescence measurements are relatively insensitive, showing changes of only ~10% for a 100-mV potential change. Thus it is a demanding task to obtain quantitative measurements with such a small dynamic range. In contrast, using a model membrane, we previously demonstrated that the SHG intensity was strongly modulated by an applied electric field (Bouevitch et al., 1993). Here we investigate the SHG

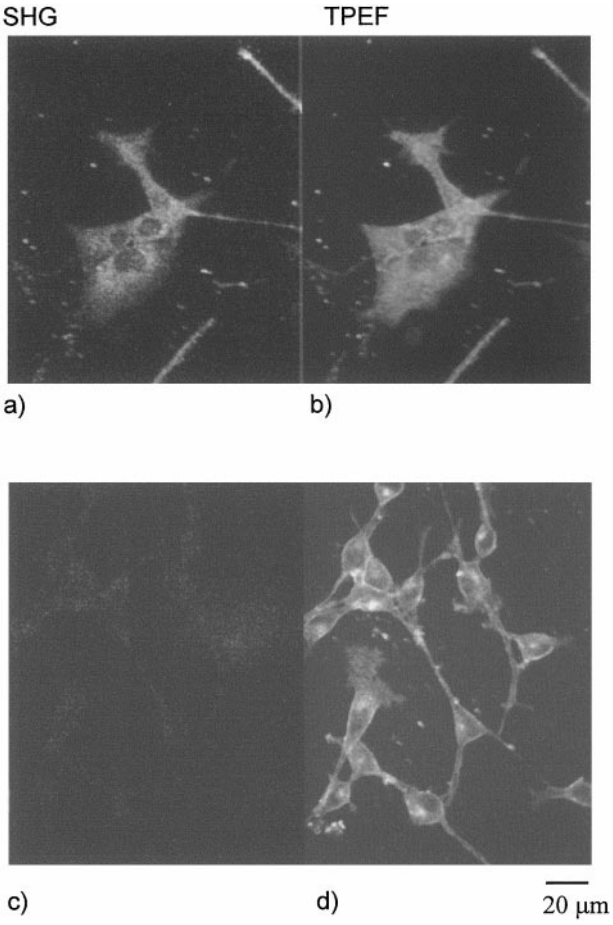

FIGURE 6 (*a*) SHG and (*b*) TPEF images of JPW-1259-stained 3T3 cells and (*c*) SHG and (*d*) TPEF images of di-4-ANEPPS-stained 3T3 cells. These images are the result of three Kalman averages and 3 s of total acquisition time.

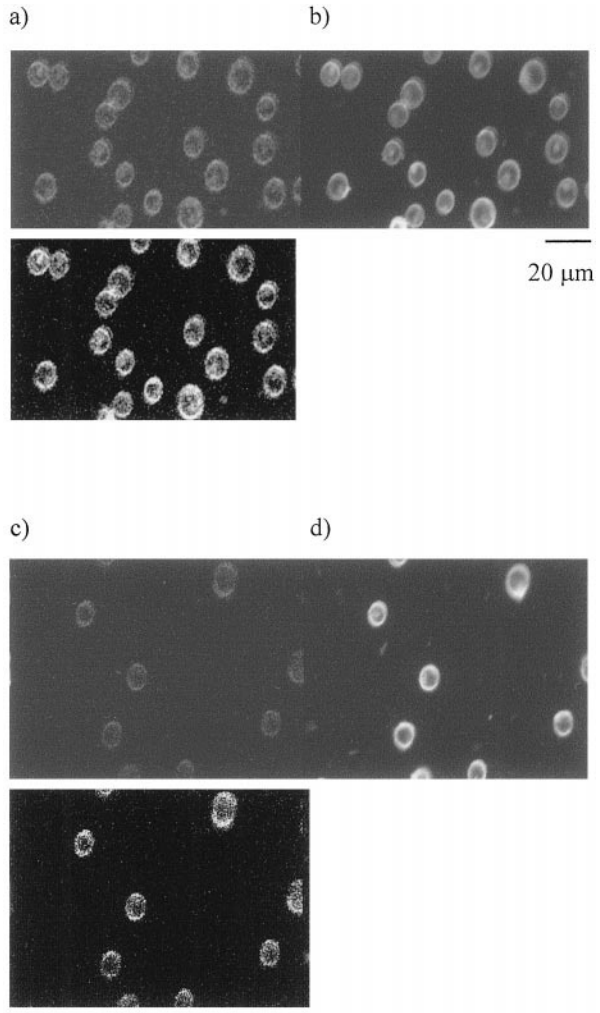

FIGURE 7 (*a*) SHG and (*b*) TPEF images of JPW-2080-stained L1210 cells in normal buffer and (*c*) SHG and (*d*) TPEF images of JPW-2080-stained L1210 cells in 135 mM K^+ buffer. These images were obtained with one scan, requiring 1 s of acquisition time. The top panels are the raw data images, and the bottom SHG panels contain the same images but have been contrast expanded for better visualization.

sensitivity to changes in membrane potential, using both a spectroscopic ensemble-averaged scheme and imaging approaches. Using the same SHG/TPEF ratiometric methodology used above, we made quantitative measurements of SHG efficiency in L1210 cell suspensions upon membrane depolarization. Measurements were performed in samples of both normal and potassium buffer (135 mM). Spectroscopic and imaging data on 30 trials showed normalized ratios,

$$\left(\frac{\text{SHG}}{\text{TPEF}}\right)_{\text{lowK}^+} : \left(\frac{\text{SHG}}{\text{TPEF}}\right)_{\text{highK}^+} \tag{4}$$

2.1 ± 0.4 and 2.3 ± 0.6, respectively. Confocal fluorescence imaging of TMRE, a Nernstian indicator (Loew, 1993, 1998), showed that this concentration of K^+ led to a depolarization of $\sim$25 mV in these cells.

The imaging data are the result of integrating intensities of individual whole cells. Representative SHG and TPEF images for these cells in low and high potassium buffer are shown in Fig. 7, *a* and *b*, and Fig. 7, *c* and *d*, respectively. The SHG images in the bottom of each panel have been contrast expanded for better visualization. Inspection of these images shows that the SHG/TPEF ratio is clearly dimmer for the cells in high-potassium buffer. These results demonstrate that membrane potential measurements using SHG can be implemented on a laser scanning microscope on physiologically relevant time scales. These results also corroborate the result from prior low-resolution work that SHG with these dyes is a more sensitive probe of membrane potential than fluorescence-based methods (Ben-Oren et al., 1996; Peleg et al., 1999).

DISCUSSION

As described in the Introduction, SHG depends on a noncentrosymmetric molecular distribution or environment. This same constraint is also operative in prohibiting signal production from two opposing interfacial regions separated

by a distance much less than the coherence length, L_c. This limit is on the order of the excitation wavelength and is approximated by

$$\Delta k \cdot L_c \approx \pi \tag{5}$$

where Δk is the difference in wave vectors between the fundamental and second harmonic wavelengths. More specifically, if both the inner and outer leaflets of a membrane are equally stained, the second harmonic waves from each leaflet will be equal and opposite in direction and sum to zero. For example, both membrane leaflets of the 3T3 cells are stained, and for cells stained with the achiral chromophore, the expectation of no net SHG is indeed observed. In contrast, inspection of L1210 cells indicated little internalization, suggesting that only the outer leaflet was stained. Consequently, strong SHG signals were obtained for staining from both the achiral and chiral dyes; still, even for L1210 cells, the chiral dyes produced twice as much SHG as the achiral analogs. We conclude from these sets of experiments that in a membrane, the presence of a chiral center relaxes the requirement of the electric dipole "selection rule" that the assembly of molecules is noncentrosymmetric.

To further understand SHIM, it is instructive to consider the size of the membranous species that may be stained with these dyes. We labeled PC liposomes with both the chiral and achiral dyes and attempted to look for SHG in the apparatus shown in Fig. 4. No measurable signal was ever observed with any of the dyes. While not monodisperse, these vesicles are generally in the size range of 20–100 nm. This size is well below the coherence length (Eq. 7), and it is thus not a surprise that no net second harmonic signal was produced, because the waves from each side would vector sum to zero. On the other hand, we did observe SHG in the suspended L1210 cells. From a macroscopic point of view, a cell suspension corresponds to a centrosymmetric environment and might not be expected to produce SHG; however, from a microscopic view the membrane of each cell is locally asymmetric. Given the ~10-μm diameter of these cells, signals from each side can add constructively. Similar behavior has also been observed for micron-size plastic beads and oil droplets (Yan et al., 1998).

Given the high sensitivity of the second harmonic signal to membrane potential, we expect SHG to be a powerful tool in probing membrane physiology. While it is not within the scope of this paper to fully elucidate the underlying theoretical basis, we can provide a physical picture of this sensitivity. The cell membrane can be considered an interface between two immiscible electrolyte solutions. From the electrochemical literature, it has been shown (Conboy and Richmond, 1997) that in such a system the total second-order response can be represented by the following expression:

$$\chi^{(2)}_{\text{total}} = \chi^{(2)}_{\text{surface}} + \chi^{(3)} E_{\text{DC}} \tag{6}$$

where $\chi^{(2)}_{\text{surface}}$ arises from the structural asymmetry of the interface, E_{DC} is a static electric field, and $\chi^{(3)}$ has the same symmetry requirements as $\chi^{(2)}$, i.e., it is restricted to the membrane. Third-order coefficients are generally on the order of four to five orders of magnitude smaller than $\chi^{(2)}$, and the second term in Eq. 8 is often negligible. However, given typical intramembrane electric fields of 10^5 V/cm, this term can become significant for a cell. It should be noted that this scenario differs markedly from that in an electric field-induced second harmonic (EFISH) experiment. In the latter, an applied electric field organizes a random distribution of molecules and is solely responsible for any observed second harmonic signal. For our case, the membrane-staining dyes have a structural alignment within the membrane in the absence of a field, as indicated by a nonzero, steady-state, field-independent, second harmonic signal.

A convenient aspect of SHIM is that fluorescent dyes can be used to generate increased contrast over endogenous species. The dyes used here, di-4-ANEPPS, JPW-1259, di-8-ANEPPS, and JPW2080, shown in Fig. 2, *a–d*, respectively, all contain the same chromophore with somewhat different appendages. This chromophore and similar analogs have been used to probe membrane potential using ratiometric fluorescence methods (Montana et al., 1989; Zhang et al., 1998). In a membrane environment, the one-photon excitation (OPE) and emission maxima are 480 nm and 650 nm, respectively. The TPE and SHG spectra are currently being measured and will be the subject of a future study. For the case of outer leaflet staining in L1210 lymphocytes we found that the sugar group increases $\chi^{(2)}$ by a factor of ~2. Overall, the second-order response (Huang et al., 1988) is an order of magnitude larger than that of rhodamine 6G (Shen, 1989), making this molecule an excellent probe for SHG studies. Recent work has also shown that supramolecular chirality can lead to significantly enhanced nonlinear optical properties (Verbiest et al., 1998).

The investigation of chemical properties leading to large second- and third-order nonlinear optical properties is currently an active area of research (Marder et al., 1989, 1991; Whitaker et al., 1996; Kenis et al., 1998; Albert et al., 1998; Tykwinski et al., 1998; Verbiest et al., 1998). While specifics vary between classes of molecules, some generalizations are becoming apparent. Typically, dyes that have extended conjugated pi networks, aromatic heteroatom (nitrogen or sulfur) substitution, and electron donor/acceptor pairs and large change in dipole moment between the ground and excited states have both large $\chi^{(2)}$ and $\chi^{(3)}$ values. The ANEPPS chromophore shown in Fig. 2 with the strongly donating dialkyamino group certainly satisfies all of these criteria. Furthermore, within the two-level system model, the second-order hyperpolarizability, β, i.e., the molecular version of $\chi^{(2)}$, and thus SHG efficiency are given by

$$\beta = \frac{3e^2}{2\hbar^3} \frac{\omega_{ge} f_{ge} \Delta\mu_{ge}}{[\omega_{ge}^2 - \omega^2][\omega_{ge}^2 - 4\omega^2]} \tag{7}$$

where e is the electron charge and ω_{ge}, f_{ge}, and $\Delta\mu_{ge}$ are the energy difference, oscillator strength, and change in dipole

moment between the ground and excited states, respectively (Tykwinski et al., 1998). A similar styryl chromophore, ASP, has a change in dipole moment of ~16 Debyes between these states (Loew and Simpson, 1981). The ANEPPS chromophore is expected to have a comparable $\Delta\mu_{ge}$, thus leading to large SHG efficiency. In addition, the two-photon absorption cross section of this chromophore is very large, $\sim 10^{-47}$ cm^4 s, which is ~20-fold larger than that of rhodamine B. Other styryl chromophores have also been reported to have large second-order nonlinear optical susceptibilities (Marder et al., 1991). These properties make styryl dyes ideal stains for both TPEF and SHIM. Native membrane proteins can also be used to produce a SHG image; for example, Alfano recently demonstrated endogenous SHG imaging of chicken muscle tissue in which an acquisition time of several hours was required to collect a single frame (Guo et al., 1997). However, cells stained with the styryl dyes used in this work are sufficiently bright to permit rapid acquisition of SHG images with low laser power.

It is straightforward to estimate the magnitude of the SHG signal. The intensity of the surface second harmonic signal per laser pulse is given by (Shen, 1989)

$$S(2\omega) = [32\pi^3\omega \sec^2\theta/\hbar c^3 \epsilon(\omega)^{1/2}(2\omega)] \cdot [L(2\omega)\chi^{(2)}L(\omega)L(\omega)]^2 I^2(\omega) AT \quad (8)$$

per pulse, where θ is the angle of incidence of the laser; $\epsilon(\omega)$ is the dielectric constant; $L(\omega)$ represents the Fresnel factor and beam polarization at ω; and $I(\omega)$, A, and T, are the intensity, cross-sectional area, and pulse width of the laser, respectively. Of particular interest are the dependencies of the SHG on peak intensity, pulse width, and angle of incidence. The signal is quadratic with peak power, but because SHG is an instantaneous process, a signal will only be generated during the duration of the laser pulse. Thus, although it is derived from different physics, SHG has the same inverse dependence on the laser pulse width as TPE fluorescence. The $\sec^2(\theta)$ dependence on the angle of incidence implies that flat samples will produce little signal at the usual laser scanning normal incidence configuration. However, cell membranes have significant curvature and thus provide good signal levels. This constraint also minimizes any SHG from the coverslip or slide. With no resonance enhancement the following signal estimate is made. For a spot size of 400 nm, 50 mW average power at the sample, 100 fs pulse duration, 76 MHz repetition rate, and an incident angle of 45°, a monolayer of styryl dye will produce a second harmonic signal of ~500 photons per pulse. Although the coverage in a membrane is hard to quantify, 1% of a monolayer is a realistic estimate. Within a pixel dwell time of 1 μs, there will be 76 pulses, and given 50% collection efficiency and 10% photomultiplier quantum efficiency, ~20 counts per pixel are expected. In these experiments, typical bright pixels in a single frame contained 5–10 detected photons, in rough agreement with this estimate. It should be noted that these numbers are only approximate because the actual conditions of coverage and incident angle and enhancement due to resonance are unknown.

Because SHG is a nonlinear optical process, SHIM retains the intrinsic advantages of multiphoton excitation fluorescence microscopy (Denk et al., 1990). Multiphoton absorption physics confines excitation to the plane of focus, greatly reducing out-of-plane photobleaching and phototoxicity. A drawback is that, per unit laser power, SHG is a less efficient process than TPEF. Furthermore, as shown earlier, SHG can be significantly resonance enhanced; however, because any ancillary TPE fluorescence comes at the expense of photobleaching, an optimal wavelength would be on the tail of an absorption band to enhance the SHG intensity while minimizing absorption. Given the flexibility of working at longer wavelengths, it may well be acceptable to use slightly higher laser power without inducing cell damage.

SHIM has the potential additional advantage that because the signal arises from an induced polarization rather than an absorption, in-plane photobleaching and toxicity can be reduced if imaging is performed off-resonance. We are currently investigating the extent of resonance enhancement in this chromophore to ascertain the viability of live-cell imaging under these conditions and are continuing work on the development of new chromophores with large second-order nonlinear susceptibilities.

CONCLUSIONS

We have shown that surface second harmonic generation is a viable contrast mechanism in laser scanning nonlinear optical microscopy; the technique has been demonstrated for three cell lines. This form of excitation maintains the advantages inherent in two- and three-photon excited fluorescence and can potentially do so without significant in-plane photobleaching and phototoxicity. We have shown that chirality of staining molecules has a pronounced effect on image formation. In addition, we have demonstrated that SHG can be used in a laser scanning microscope to measure membrane potential at a much higher sensitivity than is possible through fluorescence, providing a powerful tool for probing physiology. These properties of SHIM thus can provide a new imaging methodology that complements existing nonlinear optical schemes.

We thank Dr. Gadi Peleg, Dr. Kurt Hoffacker, Prof. Gary Leach, and Prof. Mark Terasaki for helpful technical discussions.

We gratefully acknowledge financial support under Office of Naval Research grant N0014-98-1-0703, National Institutes of Health, National Institute of General Medical Sciences 5 R01-GM35063, the National Science Foundation Academic Research Infrastructure DBI-9601609, and the State of Connecticut Critical Technology program.

REFERENCES

Albert, I. D. L., T. J. Marks, and M. A. Ratner. 1998. Remarkable NLO resonse and infrared absorption in simple twisted molecular π-chromophores. *J. Am. Chem. Soc.* 120:11174–11181.

Ben-Oren, I., G. Peleg, A. Lewis, B. Minke, and L. Loew. 1996. Infrared nonlinear optical measurements of membrane potential in photoreceptor cells. *Biophys. J.* 71:1616–1620.

Bouevitch, O., A. Lewis, I. Pinevsky, J. P. Wuskell, and L. M. Loew. 1993. Probing membrane potential with non-linear optics. *Biophys. J.* 65: 672–679.

Conboy, J. C., and G. L. Richmond. 1997. Examination of the electrochemical interface between two immiscible electrolyte solutions by second harmonic generation. *J. Phys. Chem. B.* 101:983–990.

Denk, W., J. H. Strickler, and W. W. Webb. 1990. Two-photon laser scanning fluorescence microscopy. *Science.* 248:73–76.

Denk, W., M. Sugimori, and R. Linas. 1995. Two types of calcium response limited to single spines in cerebellar Purkinje cells. *Proc. Natl. Acad. Sci. USA.* 92:8279–8282.

Eisenthal, K. B. 1996. Liquid interfaces probed by second-harmonic and sum-frequency spectroscopy. *Chem. Rev.* 96:1343–1360.

Gauderon, R., P. B. Lukins, and C. J. R. Sheppard. 1998. Three-dimensional second harmonic generation imaging with femtosecond laser pulses. *Optics Lett.* 23:1209–1211.

Gu, M., and C. J. R. Sheppard. 1995. Comparison of three-dimensional imaging properties between two-photon and single-photon fluorescence microscopy. *J. Microsc.* 177:128–137.

Guo, Y., P. P. Ho, H. Savage, D. Harris, P. Sacks, S. Schantz, F. Liu, N. Zhadin, and R. R. Alfano. 1997. Second-harmonic tomography of tissues. *Optics Lett.* 22:1323–1325.

Heinz, T. F., C. K. Chen, D. Ricard, and Y. R. Shen. 1982. Spectroscopy of molecular monolayers by resonant second-harmonic generation. *Phys. Rev. Lett.* 48:478–481.

Hell, S., M. Schrader, and H. T. M. van der Voort. 1997. Far-field fluorescence microscopy with three-dimensional resolution in the 100-nm range. *J. Microsc.* 187:1–7.

Hellwarth, R., and P. Christensen. 1974. Nonlinear optical microscopic examination of structure in polycrystalline ZnSe. *Optics Commun.* 12: 318–322.

Huang, Y., A. Lewis, and L. M. Loew. 1988. Non-linear optical properties of potential sensitive styryl dyes. *Biophys. J.* 53:665–670.

Kenis, P. J. A., O. F. J. Noordman, S. Houbrechts, G. J. van Hummel, S. Harkema, F. C. J. M. Veggel, K. Clays, J. F. J. Engbersen, A. Persoons, N. F. van Hulst, and D. N. Reinhoudt. 1998. Second-order nonlinear optical properties of the four tetranitrotetrapropoxycalix[4]arene conformers. *J. Am. Chem. Soc.* 120:7875–7883.

Kleinfeld, D., P. P. Mitra, F. Helmchen, and W. Denk. 1998. Fluctuations and stimulus-induced changes in blood flow observed in individual capillaries in layers 2 through 4 of rat neocortex. *Proc. Natl. Acad. Sci. USA.* 95:15741–15746.

König, K., T. W. Becker, P. Fischer, I. Riemann, and K.-J. Halbhuber. 1999. Pulse-length dependence of cellular response to intense near-infrared laser pulses in multiphoton microscopes. *Optics Lett.* 22: 113–115.

König, K., P. T. C. So, W. W. Mantulin, and E. Gratton. 1997. Cellular response to near-infrared femtosecond laser pulses in two-photon microscopes. *Optics Lett.* 22:135–136.

Lewis, A., A. Khatchatouriants, M. Treinin, Z. Chen, G. Peleg, N. Friedman, O. Bouevitch, Z. Rothman, L. Loew, and M. Sheves. 1999. Second harmonic generation of biological interfaces: probing the membrane protein bacteriorhodopsin and imaging membrane potential around GFP molecules at specific sites in neuronal cells of C. Elegans. *Chem. Phys.* 245:133–144.

Loew, L. M. 1993. Confocal microscopy of potentiometric fluorescent dyes. *Methods Cell Biol.* 38:194–209.

Loew, L. M. 1994. Voltage-sensitive dyes and imaging neuronal activity. *Neuroprotocols.* 5:72–79.

Loew, L. M. 1998. Measuring membrane potential in single cells with confocal microscopy. *In* Cell Biology: A Laboratory Handbook, Vol. 3. J. E. Cellis, editor. Academic Press, Orlando, FL. 375–379.

Loew, L. M., and L. Simpson. 1981. Charge shift probes of membrane potential. A probable electrochromic mechanism for ASP probes on a hemispherical lipid bilayer. *Biophys. J.* 34:353–365.

Maiti, S., J. B. Shear, R. M. Williams, W. R. Zipfel, and W. W. Webb. 1997. Measuring serontonin distribution in live cells with three-photon excitation. *Science.* 275:530–532.

Maletic-Savatic, M., R. Malinow, and K. Svoboda. 1999. Rapid dendritic morphogenesis in CA1 hippocampal dendrites induced by synaptic activity. *Science.* 283:1923–1927.

Marder, S. R., D. N. Beratan, and L.-T. Cheng. 1991. Approaches for optimizing the first electronic hyperpolarizability of conjugated organic molecules. *Science.* 252:103–106.

Marder, S. R., J. W. Perry, and W. P. Schaeffer. 1989. Synthesis of organic salts with large second-order optical nonlinearities. *Science.* 245: 626–628.

Montana, V., D. L. Farkas, and L. M. Loew. 1989. Dual wavelength ratiometric fluorescence meaurements of membrane potential. *Biochemistry.* 28:4536–4539.

Niswender, K. D., S. M. Blackman, L. Rohde, M. A. Magnuson, and D. W. Piston. 1995. Quantitative imaging of green fluorescent protein in cultured cell: comparison of microscopic techniques, use in fusion proteins, and detection limits. *J. Microsc.* 180:109–116.

Patterson, G. H., S. M. Knobel, W. D. Sharif, S. R. Kain, and D. W. Piston. 1997. Use of the green fluorescent protein and its mutants in quantitative fluorescence microscopy. *Biophys. J.* 73:2782–2790.

Peleg, G., A. Lewis, M. Linial, and L. M. Loew. 1999. Non-linear optical measurement of membrane potential around single molecules at selected cellular sites. *Proc. Natl. Acad. Sci. USA.* 96:6700–6704.

Potter, S. M., C.-M. Wang, P. A. Garrity, and S. E. Fraser. 1996. Intravital imaging of green fluorescent protein using two-photon laser-scanning microscopy. *Gene.* 173:25–31.

Shen, Y. R. 1989. Surface properties probed by second-harmonic and sum-frequency generation. *Nature.* 337:519–525.

Sheppard, C. J. R., R. Kompfner, J. Gannaway, and D. Walsh. 1977. Scanning harmonic optical microscope. *IEEE J. Quantum Electron.* 13E:100D.

Tykwinski, R. R., U. Gubler, R. E. Martin, F/Diederich, C. Bosshard, and P. Gunter. 1998. Structure-property relationships in third-order nonlinear optical chromophores. *J. Phys. Chem. B.* 102:4451–4465.

Verbiest, T., S. V. Elshocht, M. Kauranen, L. Hellemans, J. Snauwaert, C. Nuckolls, T. J. Katz, and A. Persoons. 1998. Strong enhancement of nonlinear optical properties through supramolecular chirality. *Science.* 282:913–915.

Whitaker, C. M., E. V. Patterson, K. L. Kott, and R. J. McMahon. 1996. Nitrogen and oxygen donor in nonlinear optical materials: effects of alkyl vs phenyl substitution on the molecular hyperpolarizability. *J. Am. Chem. Soc.* 118:9966–9973.

Wokosin, D. L., V. E. Centonze, S. Crittenden,, and J. White. 1996. Three-photon excitation fluorescence imaging of biological specimens using an all-solid state laser. *Bioimaging.* 4:208–214.

Yan, C. Y., Y. Liu, and K. B. Eisenthal. 1998. New method for determination of surface potential of microscopic particles by second harmonic generation. *J. Phys. Chem. B.* 102:6331–6336.

Zhang, J., R. M. Davidson, M. Wei, and L. M. Loew. 1998. Membrane electrical properties by combined patch clamp and fluorescence ratio imaging in single neurons. *Biophys. J.* 74:48–53.